

Exploring the Land–Ocean Contrast in Convective Vigor Using Islands

F. J. ROBINSON

Department of Geology and Geophysics, Yale University, Connecticut

S. C. SHERWOOD

Climate Change Research Centre, University of New South Wales, Sydney, Australia

D. GERSTLE

Department of Geology and Geophysics, Yale University, Connecticut

C. LIU

Department of Atmospheric Sciences, University of Utah, Salt Lake City, Utah

D. J. KIRSHBAUM

Department of Meteorology, University of Reading, Reading, United Kingdom

(Manuscript received 20 May 2010, in final form 9 August 2010)

ABSTRACT

Moist convection is well known to be generally more intense over continental than maritime regions, with larger updraft velocities, graupel, and lightning production. This study explores the transition from maritime to continental convection by comparing the trends in Tropical Rainfall Measuring Mission (TRMM) radar and microwave (37 and 85 GHz) observations over islands of increasing size to those simulated by a cloud-resolving model. The observed storms were essentially maritime over islands of $<100 \text{ km}^2$ and continental over islands $>10\,000 \text{ km}^2$, with a gradual transition in between.

Equivalent radar and microwave quantities were simulated from cloud-resolving runs of the Weather Research and Forecasting model via offline radiation codes. The model configuration was idealized, with islands represented by regions of uniform surface heat flux without orography, using a range of initial sounding conditions without strong horizontal winds or aerosols. Simulated storm strength varied with initial sounding, as expected, but also increased sharply with island size in a manner similar to observations. Stronger simulated storms were associated with higher concentrations of large hydrometeors. Although biases varied with different ice microphysical schemes, the trend was similar for all three schemes tested and was also seen in 2D and 3D model configurations. The successful reproduction of the trend with such idealized forcing supports previous suggestions that mesoscale variation in surface heating—rather than any difference in humidity, aerosol, or other aspects of the atmospheric state—is the main reason that convection is more intense over continents and large islands than over oceans.

Some dynamical storm aspects, notably the peak rainfall and minimum surface pressure low, were more sensitive to surface forcing than to the atmospheric sounding or ice scheme. Large hydrometeor concentrations and simulated microwave and radar signatures, however, were at least as sensitive to initial humidity levels as to surface forcing and were more sensitive to the ice scheme.

Issues with running the TRMM simulator on 2D simulations are discussed, but they appear to be less serious than sensitivities to model microphysics, which were similar in 2D and 3D. This supports the further use of 2D simulations to economically explore modeling uncertainties.

1. Introduction

Understanding and quantitatively predicting deep convection continues to be a central challenge in atmospheric sciences (Arakawa 2004; Stevens 2005). Warm-season

Corresponding author address: F. J. Robinson, Department of Geology and Geophysics, Kline Geology Laboratory, P.O. Box 208109, Yale University, New Haven, CT 06520–8109.
E-mail: frank.robinson@yale.edu

storm activity remains difficult to predict (Fritsch and Carbone 2004), and different representations of convection in climate models continue to produce substantially different simulations, even of the general circulation (e.g., Bacmeister et al. 2006; Zhang et al. 2007). The solution of this problem remains one of the most important in atmospheric sciences.

Desperation has led some groups to replace the traditional cumulus parameterization in global models with explicit cloud-resolving models (CRMs)¹ running inside each grid cell of the global model, the so-called multi-scale modeling framework (MMF). This has improved some aspects of global simulations (e.g., Pritchard and Somerville 2008; Stan et al. 2010), but at great computational expense. The use of CRMs is not a panacea: for example, problems can persist in the seasonal cycle of convective cloud and water vapor over land (Zhang et al. 2008), errors typically blamed on convective schemes. This highlights the possibility that CRMs, though better than traditional parameterizations (e.g., Xu et al. 2002), still may make systematic errors that affect climate simulations. One problem is that CRMs at 1-km or even 500-m resolution explicitly resolve only a small part of the full spectrum of convective turbulence, with the smaller scales requiring parameterization. Updrafts therefore tend to be unrealistically laminar. Another problem is that CRMs require detailed treatments of complex microphysical processes, and different representations of this can lead to storms that even have different dynamical structure (e.g., Li et al. 2009). Finally, there are uncertainties in how to treat the boundary layer where relatively small-scale motions eventually give rise to deep convection.

It has been difficult to test CRMs because of observational limitations. For example, storm development is very sensitive to environmental conditions that are hard to measure such as flow divergence, small-scale details at low levels (e.g., Wakimoto and Murphey 2008; Wilson and Schreiber 1986), or small variations in convective instability (Lima and Wilson 2008). More fundamentally, chaotic turbulent phenomena can be expected to evolve differently over time even with nearly identical initial conditions and forcings. Finally, important storm characteristics such as ice content and vertical velocities are observed only in limited circumstances. Even in field programs, it can be difficult to distinguish which of two rather different storm simulations is more accurate (Li et al. 2009). For all these reasons it is difficult to falsify

a CRM from its simulation of an individual storm, although simulated radar signatures can sometimes fall well outside a realistic range (Li et al. 2008; Zhou et al. 2007), indicating far too many large particles at upper levels.

The above concerns all suggest that we should test CRMs in other ways. One exciting but expensive option is to use a global cloud-system-resolving model to simulate the entire atmosphere and compare various aspects of the results directly to global observations (Inoue et al. 2010). Alternatively we can perform many runs on a limited scale and evaluate systematic variations or trends in the simulations. First, by averaging over many convective events one can beat down the noise associated with unobservable details or stochastic behavior and reveal model errors that would not be detectable in a single event. Second, contrasting results in different forcing situations can reveal aspects that are more important to the interaction of convection with larger scales.

Several previous studies have followed this strategy. J. Wu et al. (2009) found that the Weather Research and Forecasting (WRF) CRM was able to simulate qualitatively the significant differences in the character of convection between active and break-monsoon convection over northern Australia. Matsui et al. (1989) compared observed and modeled storm characteristics in the South China Sea Monsoon Experiment (SCSMEX) and the Kwajalein Experiment (KWAJEX), finding that peak SCSMEX storms reached higher in both observations and two CRMs tested. Unfortunately, differences in other indicators of storm intensity, such as radar retrievals at middle and lower levels or microwave brightness temperatures, were generally not captured by either CRM. This could be due to model biases or errors in the prescribed forcing, as suggested by Matsui et al. (1989). Systematic comparisons with regime-sorted field data (Marchand et al. 2009a) and with global statistics from satellite data (Marchand et al. 2009b) show that MMF simulations appear to be accurate for dynamically forced cloud bands such as those associated with cool-season frontal systems, while systematically overestimating upper-level cloud and low-level precipitation in more convective or warm-season settings.

Perhaps the single most evident systematic variation in convection is the simple contrast between land and ocean. Continental storms are often highly electrified and have the most extreme microwave and radar signatures, whereas lightning is rare over oceans (Zipser et al. 2006). This contrast is not easy to explain: it is likely due to much stronger updrafts in continental storms, but it is not obvious why continental updrafts should be stronger and multiple explanations have been offered

¹ In some cases the resolution is not really sufficient to resolve clouds properly and "cloud-permitting models" would be more accurate.

(Sherwood et al. 2006; Zipser and Lutz 1994). Factors that have been suggested include higher CAPE, thicker continental boundary layers, orographic lifting, and aerosol nucleation effects. We have not found any CRM study that has directly tested the ability of CRMs to explain these land–ocean contrasts based on any of these factors.

An interesting way to gain leverage may be to look at island convection. Past studies (Kirshbaum and Smith 2009; Smolarkiewicz et al. 1988; Yu and Cheng 2008) have often focused on the role of orography in generating convection over islands in the presence of a background wind, but in this study we focus on the role of diurnal heating in generating convection. A prime example where this is important is the Tiwi Islands with their famous Hector storms, of which there have been both simulations (Chemel et al. 2009; Connolly et al. 2006; Crook 2000; Saito et al. 2001) and observational studies (Schafer et al. 2001). Carbone et al. (2000) categorized Hectors into two main types, one (comprising 80% of cases) a result of gust front–sea breeze interactions and the other a result of merging sea breezes. Island convection is characterized by low-level moisture, which plays a vital role in controlling the convective organization and strength, particularly if the surface winds are weak (Crook 2000), so that low-level air spends more time over the heated island, allowing moist instability to grow.

Previous work has shown that the electrification of convection over islands transitions smoothly from maritime to continental as the size of the islands increases, with much of the increase in electrification occurring at island sizes near a few thousand square kilometers (Williams and Stanfill 2002). A previous study (Robinson et al. 2008, hereafter RSL08) found that variations in the depth of the heat low in surface pressure associated with convection similar to the observed lightning variations could be explained by linear dynamics, where excitation of the system at horizontal scales below a resonant scale would not permit the efficient generation of a forced gravity wave response and, therefore, would produce weak convection. That study was unable to directly compare simulations to observations since lightning was not simulated by the model.

Here we extend the RSL08 study by quantitatively testing the trends in WRF model simulations over various island sizes against observations. We do this by comparing simulated and observed microwave and radar signatures of convection, obtaining observations from the Tropical Rainfall Measuring Mission (TRMM) satellite, and generating simulated observations using offline radiative transfer codes. The sensitivity of the results to microphysics will be tested, and to account for atmospheric

variability we simulate behavior under a range of environmental initial conditions for each island size, using more realistic forcing conditions than in RSL08. Model islands are heated regions within a flat uniform terrain of finite extent. Since two-dimensional simulations are much more affordable for exploring the range of influences on simulated convection, we conduct the bulk of our simulations in two dimensions, but also explore the relationships between 2D and 3D simulations as viewed by TRMM, and show how 2D simulations may be approximately compared with real-world TRMM observations.

The main goal of this work is to explain the observed increase in storm strength from maritime to continental environments. By investigating with idealized boundary conditions and similar initial conditions across all simulations, we will test to what extent the trend can be attributed to the horizontal heterogeneity of thermal surface forcing, as suggested by RSL08, rather than background humidity, boundary layer depth, aerosols, onshore advection of colder marine air by strong trade winds, or other factors that might be implicated in explaining the continent/ocean difference. We will also be able to quantify the impacts of different microphysical schemes or atmospheric soundings on means and trends. A second goal of the study will be to test how well the WRF model and a simulator are, together, able to simulate behavior in 2D versus 3D configurations. We will show that both 2D and 3D models are able to satisfactorily reproduce observed trends in convective strength, affirming the utility of satellite simulators even in two dimensions.

2. Observational study: TRMM dataset

The TRMM satellite is a nongeosynchronous weather satellite, with inclination of 35°, which was launched in November 1997 with the purpose of measuring rainfall and energy exchange in tropical and subtropical regions (Kummerow et al. 1998). To this end, it is equipped with the TRMM Microwave Imager (TMI) for total precipitation rates, Precipitation Radar (PR) for vertical distribution of precipitation sized particles, the Visible and Infrared Radiometer System (VIRS) for temperature and peak altitude of clouds, and the Lightning Imaging Sensor (LIS) for detecting lightning (Kummerow et al. 1998).

To compare CRM simulations to TRMM observations, the University of Utah Precipitation Feature database (Liu et al. 2008) was used. This database includes the raining precipitation features (RPFs) defined by grouping areas with TRMM PR 2A25 nonzero rainfall (Iguchi et al. 2000). From January 1998 through December 2007, the database contains over two million

snapshots of RPFs with size greater than 80 km^2 . Various characteristics of PR, TMI, VIRS, and LIS observations within each RPF are summarized. The database also provides a sounding for each RPF, taken from the nearest point in the National Centers for Environmental Prediction (NCEP)–National Center for Atmospheric Research (NCAR) reanalysis. In this study we focus on the maximum height of PR 40-dBZ radar echoes and the minimum polarization corrected temperature (PCT) (Spencer et al. 1989) seen by the TMI 37- and 85-GHz channels. Previous studies have found these three quantities to be useful proxies for convective intensity (Zipser et al. 2006).

To compare with simulations over islands, we selected 162 islands from the 1548 islands between 35°S and 35°N having a known area in the island directory of the United Nations Environment Programme (UNEP) (Dahl 1986, 1991; see <http://islands.unep.ch/isldir.htm>). We included all of the islands from Williams and Stanfill (2002) that were within the TRMM swath, the rest being selected at random. The islands range in size from 0.3 km^2 (Agalega, Mauritius) to $748\,168.1 \text{ km}^2$ (Borneo, Indonesia/Malaysia/Brunei).

To determine which storms in the TRMM database to identify with each island, we drew polygons around each island using the Google Earth tool (assuming Euclidean geometry and allowing for up to 47 vertices to define an island). A RPF in the TRMM database with a feature centroid falling within any island's polygon was identified as occurring over that island. We calculated statistics for all RPFs over an island, and separately for the subset of RPFs that occurred during "afternoon," which was defined as between 1200 and 1800 LT. We hypothesize that these afternoon RPFs are more likely to have formed over the island because of local surface heating, as opposed to storms forming elsewhere that drift over the island and may not be equally affected by the local affects of the island.

3. WRF model setup

We ran WRF version 3.1 (Skamarock et al. 2008) in both 2D and 3D configurations. The 2D computational domain is 600 km horizontally and 25 km vertically, with open and rigid boundaries respectively, Rayleigh damping in the uppermost 6 km, and a free-slip surface. The grid has 100-m vertical spacing and 500-m horizontal spacing in most runs. The 3D runs use the same vertical grid but 1-km horizontal resolution (the most that could be afforded). The 3D domain is a "bowling alley" with 600-km extent and open boundaries in the x direction (duplicating the 2D conditions) and 60-km extent with periodic boundary conditions in the y direction. This

affordably permits full three-dimensional turbulence at the cloud scale, though constraining motions and mesoscale and longer scales to be quasi-two-dimensional. To help initiate 3D turbulence we applied random thermal perturbations to the initial condition. The relatively large (or in 3D, long) domain was required to ensure that the dynamics was not significantly affected by boundary effects, even for the largest islands (numerical tests showed there was no significant difference between using a 600- and 1200-km x domain). The choice of 2D resolution was based on previous modeling studies (RSL08; Robinson and Sherwood 2006).

The only parameterization used in the runs is the turbulent kinetic energy (TKE) scheme (Soong and Ogura 1980) to model transport of momentum and heat at the subgrid scale. For simplicity we did not activate the additional planetary boundary layer (PBL) parameterization for representing microscale processes in the boundary layer. Numerical tests showed that the overall trends presented in this paper would not be significantly affected by including the PBL scheme.

We ran WRF with several different ice microphysical schemes to test the robustness of our results. The default is the Morrison two-moment scheme (Morrison and Pinto 2005), which has been shown to produce reasonable simulations of deep convective squall lines (Morrison et al. 2009) and in preliminary tests with our model setup yielded what appeared subjectively to be the most realistic storms. We also tested the Thompson single-moment scheme (Thompson et al. 2004), which was developed more with winter storm characteristics in mind but has been used, for example, by Khain and Lynn (2009) to simulate a supercell thunderstorm. Two-moment schemes better simulate the changes in size spectrum between convective and stratiform portions of a storm, which among other things can reduce the intensity of convective cores relative to single-moment schemes (Morrison et al. 2009); on the other hand, the Thompson scheme has been uniquely designed to mimic some of the features of bin microphysical schemes (Khain and Lynn 2009; Thompson et al. 2004). Finally, we tested the Lin scheme (Lin et al. 1983), a much older and well-known scheme used in many CRMs (incorporating a bug fix reported by NCAR on 16 October 2008). All schemes predict ice, snow, graupel, and rain mixing ratios with predicted or assumed size distributions. In a previous intercomparison, J. Wu et al. (2009) found that the Morrison scheme produced realistic graupel amounts in a tropical storm, while the Thompson scheme produced too little and the Lin scheme produced too much. Thus, the use of these alternate schemes should be helpful in assessing the sensitivity of our results to microphysical uncertainties.

To represent the effect of an island, diurnal thermal forcing is represented in an idealized way by imposing a “top-hat” sensible heat flux (horizontally uniform within a specified distance of the center of the domain) varying sinusoidally in time with a 24-h period and maximum of 200 W m^{-2} , beginning at zero and peaking six hours into the simulation. To isolate the impacts of differential heating and reduce the number of arbitrary parameters, the surface moisture (latent heat) flux was set to zero.

Under the imposed fluxes, the near-surface air temperature is predicted explicitly by the model and should be checked for realism. The simulated warming over the first 6 h was about 3.5 K, consistent with the change in surface temperature observed by the Moderate Resolution Imaging Spectroradiometer (MODIS) over Melville Island during the monsoon.² In the 3D runs, the heating was applied at all y values up to the periodic boundaries, thus forming an infinite heated “ridge” in the y direction and mimicking the 2D forcing.

a. Initial condition set

Many observational and numerical studies of convection show that the convective initiation and response is sensitive to changes in low-level wind shear and moisture (e.g., Sherwood et al. 2010; Wissmeier and Goler 2009). Thus, to obtain a representative result for a given model configuration or surface forcing that can be compared with observed statistics, a suite of simulations with a representative variation of sounding conditions must be performed. In principle one could also apply varying horizontal or vertical advection, but for simplicity and because of lack of data on this, we initialized all runs with horizontally uniform wind and thermodynamic soundings and zero vertical velocity.

To efficiently and simply span the range of sounding conditions, we formulated six soundings from the 405 reanalysis soundings (see section 2) collocated with TRMM-observed storms over Melville Island. Each of the six soundings was formulated to have a very low or high value of some chosen index expected to affect convection. First, we found low and high humidity profiles by computing the mean humidity profile of all soundings having a 500-hPa relative humidity at the 90th percentile or higher (designated HIRH), and similarly for those at

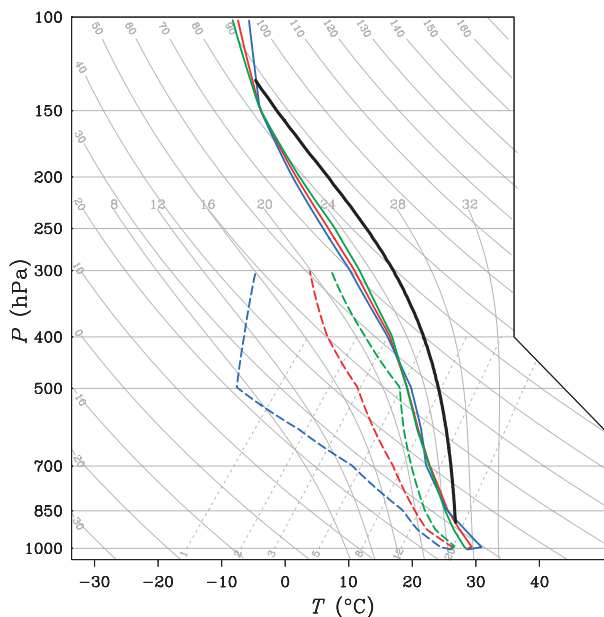


FIG. 1. Skew T - $\log p$ diagrams of temperature (solid) and dewpoint (dashed) profiles for the LOWRH (blue) and HIRH (green) soundings; the mean humidity profile used in the remaining soundings is in red. A temperature profile of an air parcel adiabatically lifted from 950 mb (380 m) is also overlaid for reference (solid black line). Note that the dewpoint profiles are only shown up to 300 mb, above which the water-vapor mixing ratio is set to zero.

or below the 10th percentile (designated LOWRH). The overall mean humidity profile was also computed and is designated MEANRH. Figure 1 shows the skew T - $\log p$ diagrams for the corresponding soundings.

We followed a similar procedure for two measures of wind shear: the shear from the surface to 1-km altitude, and that to 6-km altitude, yielding two low-shear (LS01 and LS06) and two high-shear (HS01 and HS06) profiles. Figure 2 shows these four wind profiles as well as the mean wind profile. To construct soundings to initialize the WRF model, we assigned the overall mean temperature profile and overall mean humidity profile (MEANRH) to the LS01/HS01/LS06/HS06 soundings and the overall mean wind profile to the HIRH/LOWRH soundings. These six selected combinations of humidity and winds were found to encompass the range of simulated responses that resulted from other permutations of these parameters (e.g., using the mean humidity along with the mean winds), so were deemed sufficient for these experiments. For 3D runs the wind shear was applied in the x direction.

This procedure involved a number of arbitrary choices and is not necessarily ideal. The focus on midlevel humidity was motivated by many recent studies showing a strong influence of this and by the robust correlation of midlevel humidity to that at other levels (Holloway and

² Based on our perusal of the level-2 surface temperature product averaged from 8 to 15 Nov 2008: *Terra* (1030 LT) MOD11A2 (min = 293.5 K, max = 317.3 K, mean = 304.3 K); *Aqua* (1330 LT) MYD11A2 (min = 289 K, max = 321.6 K, mean = 306.9 K). The increase of 2.6 K between 1030 and 1330 LT is roughly consistent with the 3.5-K increase found here in 6 h.

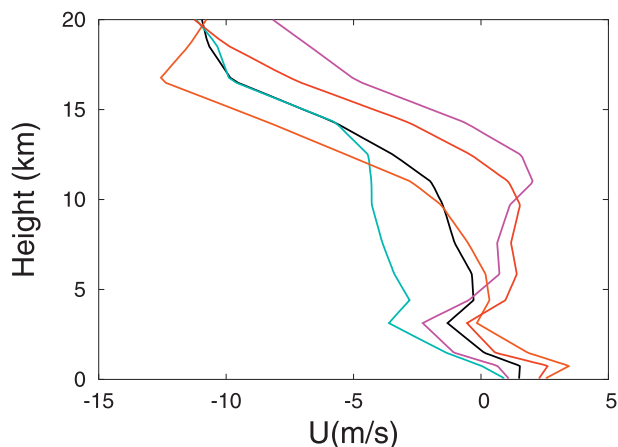


FIG. 2. Background wind for the 2D simulations: HS01 (pink), LS01 (orange), HS06 (light blue), and LS06 (red). The overall mean wind profile (used in the LOWRH and HIRH soundings) is shown in black.

Neelin 2009). The importance of 6-km or “deep” shear has been emphasized by many previous studies going back to Moncrieff and Green (1972). Our choice of 1-km shear is more unconventional but was motivated by some preliminary tests showing this to affect convection, and by previous studies showing that it affects severe storm characteristics (see Brooks 2009). The resulting soundings all have a CAPE of 240 J kg^{-1} , except for LOWRH (0 J kg^{-1}) and HIRH (400 J kg^{-1}), which differ due to the varying boundary layer relative humidity. Of course, the CAPE in the domain center increases during the simulation because of surface heating.

For simplicity, in our examination of trends with island size we used the same set of six soundings for all island sizes. The soundings in the RPF database showed

no evidence that CAPE, humidity, or any other aspect examined was correlated with island size (there was a slight decline in CAPE with increasing size but this was insignificant). Trends in convective behavior therefore would not have been significantly different if we had followed a more complicated procedure of adopting different initial soundings for each island. Note, however, that other possible atmospheric characteristics such as initial cloud cover, wave activity, or aerosol concentrations, which were simply neglected or held at default values for all of our simulations, could potentially have trends with island size.

b. Simulated storm characteristics

The simulated storms consistently follow certain patterns. After a few hours the land–sea temperature contrast is large enough for sea breeze fronts to start moving inward from the “coasts” (edges of the hot spots). The fronts move inward, colliding near the center and producing a strong burst of convection. The speed of these fronts is sometimes altered by gusts caused by evaporative cooling of precipitation.

To illustrate this development, we show simulations for an 80-km island with the HS01 sounding (a case that produces an intermediate convective response). Two snapshots of the temperature perturbation (effectively the buoyancy) are shown in Fig. 3. In this case convection was initially triggered at the coasts (not shown), which for an 80-km island are located at 10 and 90 km in the 100-km subdomain. The first figure shows the location of the fronts at 6 h 37 min; the second figure shows the burst of convection that follows soon after, once the fronts collide. (The corresponding time series of 85-GHz PCT for this case appears in Fig. 7d.) The generation of strong

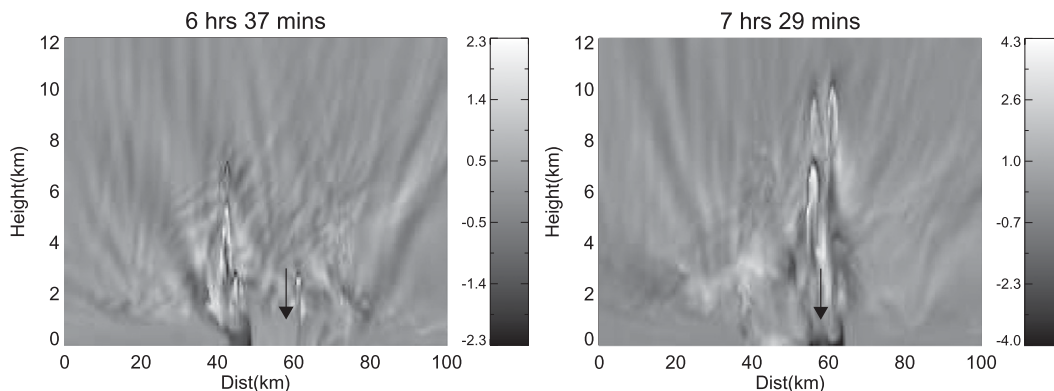


FIG. 3. Snapshots of temperature perturbation (hourly mean subtracted) across the central 100 km of the model domain, (left) about 30 min before and (right) 20 min after the collision of two sea breeze fronts indicated by black arrows in the left panel. (The front indicated near $x = 47 \text{ km}$ is a combined sea breeze–gust front, whereas that near $x = 61 \text{ km}$ is a pure sea breeze front.) The collision results in a strong convective burst. The case shown is with sounding HS01, 80-km heating, and Thompson microphysics (see Fig. 7d for the time series of minimum 85-GHz PCT for this case) but the behavior shown is typical of many cases.

convection by sea breeze or gust fronts is a characteristic feature of convection over Melville Island (Carbone et al. 2000; Chemel et al. 2009), the Florida peninsula (Kingsmill 1995), and other similar-scale land features.

Many interesting questions are raised by this behavior, including the dynamics of the breeze fronts and the possible relationship of these dynamics to the free-tropospheric wave dynamical mechanisms highlighted by RSL08. These will be explored in a separate article.

c. *Satellite simulator code*

To compare WRF simulations with the TRMM dataset we ran WRF model data through version 1 of the Satellite Data Simulator Unit (SDSU) (<http://precip.hyarc.nagoya-u.ac.jp/sdsu/sdsu-main.html>) (Masunaga et al. 2010). The microwave radiometer simulator part was based on Kummerow (1993) and the radar simulator on Masunaga and Kummerow (2005). For snow, graupel, and rain, SDSU assumes an exponential distribution with user-provided water content and internally prescribed density and “intercept” parameter (a parameter governing the total number concentration). For ice, SDSU fits to the observed cloud ice distributions by Heymsfield and Platt (1984).

We used the same parameters in SDSU as in WRF whenever possible. The mass–diameter relation for snow assumed by WRF–Thompson was tested in SDSU and yielded essentially identical results to the relation assumed in SDSU, so we retained the SDSU relation for all schemes. Both the Thompson and Morrison schemes admit variable intercept parameters, which is not permitted in this version of SDSU; we used central estimates of these parameters but found that reasonable variations in parameters did not make a large difference.

After reading in the WRF data and performing the radiative transfer computation, the simulator code does a beam averaging over the ground footprint. The ground footprints of the TMI (Kummerow et al. 1998) instrument are $6.8 \text{ km} \times 4.2 \text{ km}$ for 85 GHz and $16 \text{ km} \times 9.7 \text{ km}$ for 37-GHz brightness temperature (down track by cross track) axis. The PR (Kummerow et al. 1998) instrument operating near 13.8 GHz has a horizontal resolution of $4.3 \text{ km} \times 4.3 \text{ km}$ and a vertical resolution of 250 m.

d. *Model sampling strategy*

The particular statistics recorded in the TRMM feature database require careful attention to how the WRF simulations are sampled. A cloudy blob found in the TRMM imagery is included as a RPF in the database if, according to the data at that time, a radar reflectivity of 10 dBZ or greater occurs somewhere in the feature. The lowest PCTs and highest dBZ heights occurring in the feature are then recorded in the database. With few

exceptions, each of the millions of RPFs in the database will be a lone snapshot of a different storm. These snapshots will be distributed uniformly/randomly over the lives of the storms from which they are taken, and over the local time of day due to the highly sun-asynchronous TRMM orbit.

By contrast, with WRF we simulate a far smaller number of storms but can “observe” each storm as often as we like. To mimic the uniform diurnal sampling of TRMM, we ran each WRF simulation for exactly 24 h and sampled uniformly over the entire run (at 4-min intervals, though the interval does not affect results as long as it is short enough to properly sample the simulations). To mimic the conditions applied for the creating of RPFs, we only retained a given sample for further use if the 10-dBZ criterion was met according to the simulator output (this condition proved similar to requiring 0.3 g m^{-3} of rainwater content). For each qualifying sample, we follow the same procedure as with the RPF database and retain the lowest PCT and highest radar heights returned by the SDSU simulator across the raining part of the domain.

The ensemble of sample values for each simulation, accumulated over a suite of simulations with all the initial soundings, may be directly compared to an ensemble of TRMM features.³ In particular, we compare the model ensemble with runs having surface heating of scale L to that of the RPFs captured by TRMM over islands of sizes near L . The observed distributions may be affected by several factors not taken into account in modeling, however, including failure of the six soundings to be equally representative of or to fully characterize conditions, influences of small-scale waves in and out of the open lateral boundaries, waves produced by land surface orographic heterogeneities or other factors not included in the model, or advection of maritime storms over an island.

4. SDSU Benchmark: Melville Island

As a first test, we compare output from convection simulated with the above soundings as initial conditions against TRMM observations from Melville Island. The choice of Melville Island is motivated by the fact that convection there has been well studied and documented (e.g., May et al. 2009; Schafer et al. 2001) and occurs consistently in the afternoon owing to mechanisms similar to those operating in our model as described in section 3b.

³ The only practical difference between the TRMM and WRF sampling is that, owing to the strong serial correlation in the 1-min model samples, the uncertainty of model-calculated statistics cannot be determined empirically via the standard error. Such estimates can, however, be made from the TRMM data.

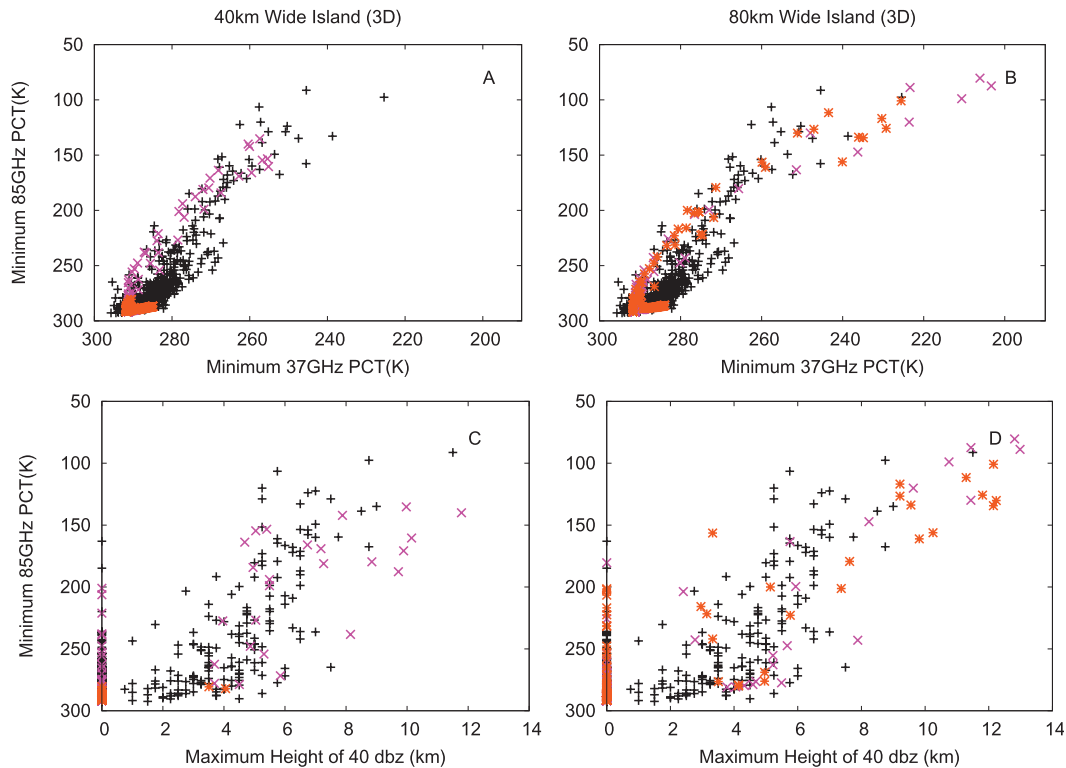


FIG. 4. Minimum 37-GHz PCT and peak 40-dBZ height, each vs minimum 85-GHz PCT. Lower PCT and higher 40-dBZ height each indicate greater lofting of large ice particles by strong convection. Each black plus sign represents a precipitation feature observed by TRMM (section 2) over Melville Island. Results from 3D WRF simulations are shown with the HS01 (pink crosses) and LS01 (orange stars) soundings, with heated patches of (a) 40 and (c) 80 km. Morrison microphysics is shown in this case. WRF-SDSU is sampled to be as equivalent as possible to TRMM (see section 3d). Note: in (a) and (c) (40-km heating) the convective response for the LS01 case is so weak that the minimum 85-GHz PCT remains close to the clear-sky value of 290 K.

We consider convection forced by idealized heated regions of 40 and 80 km, bracketing the ~ 50 -km width of the actual island.

a. Evaluation of 3D simulations

Figure 4 compares the observed and simulated minimum 37-GHz PCTs and maximum 40-dBZ heights with the minimum 85-GHz PCT for two soundings (HS01 and LS01) and two heating sizes (40 and 80 km). These simulations use the Morrison microphysics scheme and are 3D. Each of these three radiometric measures is sensitive to large ice particles lofted to high levels in the storm, a hallmark of strong storms. The 40-dBZ radar echo is an indicator of very large ice and often does not occur at all in a raining storm (yielding many heights of zero in our plots). The microwave temperatures are lower when more ice is present: the 85-GHz channel is especially sensitive to this, while the 37-GHz channel receives less scattering due to the longer wavelength but receives some emission from low levels and is affected by liquid water amounts.

The comparison shows that each of the three simulated intensity measures depends on the sounding and the surface forcing, in some cases showing a distribution similar to the observations. Moreover, the relationships among the three quantities are consistent regardless of the sounding or surface forcing (this is also true for the other initial soundings; not shown) and are encouragingly close to the observed relationships. The main differences between runs are shifts of all three measures toward more or less severe values. The difference in response over different island sizes is examined further in section 5.

Some TRMM versus WRF-SDSU discrepancies are apparent, however. While the peak intensities are similar, there are more modest-intensity points in the observations than in the simulations. These modest-intensity points also have a much tighter 85–37-GHz relation in the model than in the observations, and their 37-GHz temperatures tend to be too high in the model. The differences may indicate cumulus congestus or weaker convective events in the data that either do not appear or quickly give way to deep convection in the simulations.

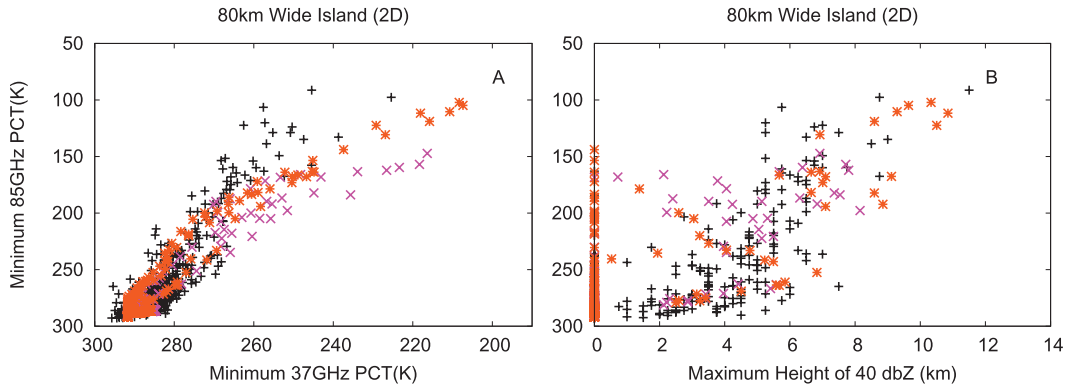


FIG. 5. As in Figs. 4b,d, but the simulations (pink and orange) are two dimensional. The horizontal SDSU footprints equal the shorter dimension of the actual TRMM TMI footprints (10 km at 37 GHz and 4 km at 85 GHz).

The scatter in observations may also reflect varying surface emissivities in the scenes observed by TRMM, which can affect the 37-GHz PCTs, and are fixed in the simulator calculations.

b. 2D simulations and beam sampling

Full 3D convection simulations are computationally expensive (both in terms of run time and storage), so to perform a large set of runs it is useful to work in 2D. While there are significant differences between 2D and 3D convection both in terms of triggering and strength of convective vigor (Avissar and Liu 1996; Petch et al. 2008), previous studies have also concluded that 2D simulations show similar sensitivities to varying conditions (e.g., C.-M. Wu et al. 2009). Unfortunately the comparison of 2D simulations with satellite data collected in a 3D world raises problems, which we now address.

For a 2D run it is not clear how wide to make the beam footprints, as there is only one horizontal dimension. Figure 5 shows the 2D equivalent results if the 2D footprints are simply made equal to the shorter length

of the actual TRMM footprint (10 and 4 km for the 37-GHz and 85-GHz PCTs, respectively, and 4.3 km for the PR radar). With these footprints, the simulated 85-GHz and radar data agree well with TRMM values, but the 37-GHz PCT is about 20–30 K lower than observed.

One explanation for the departure of the 37-GHz results is that the footprint is too small. Comparing the areas of the actual TRMM footprints, the 37-GHz channel footprint covers about 6 times the area of the 85-GHz or radar ones. But in 2D the footprint area is identical to the length, so our effective area ratio is only 2.5. Thus, depending on how the microscale cloud turbulence scales in 2D and 3D, it could be appropriate to use a 2D footprint for each channel that grows faster than the linear dimension of the actual footprint. In the limiting case of area scaling, keeping 4-km footprints for the other two quantities, we would need a 24-km 2D footprint for the 37-GHz pseudochannel. The results for these footprints are shown in Fig. 6a. Comparing this with Fig. 5a shows that results are indeed sensitive to the footprint size.

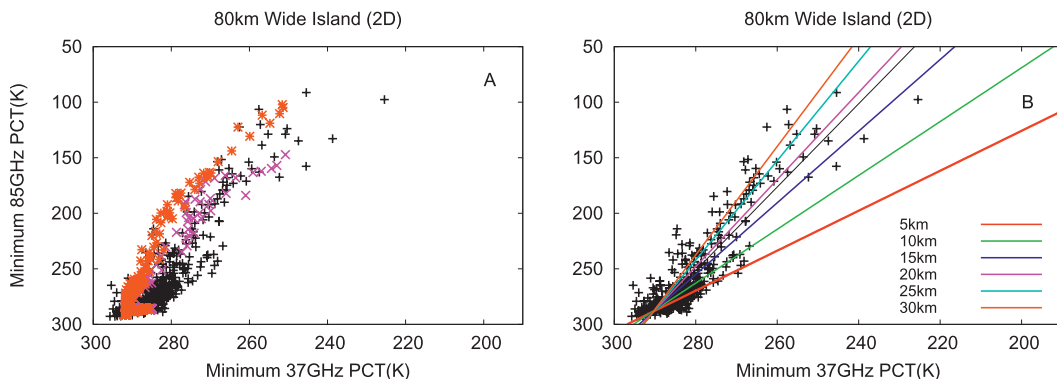


FIG. 6. (a) As in Fig. 5a, but with a larger 22-km horizontal footprint for the 37-GHz channel. (b) Results applying a range of 37-GHz footprint sizes in SDSU to 2D simulations for the HS01 sounding, indicated in colors (see legend) using best-fit lines. The fit to observations is indicated in (b) by the black line.

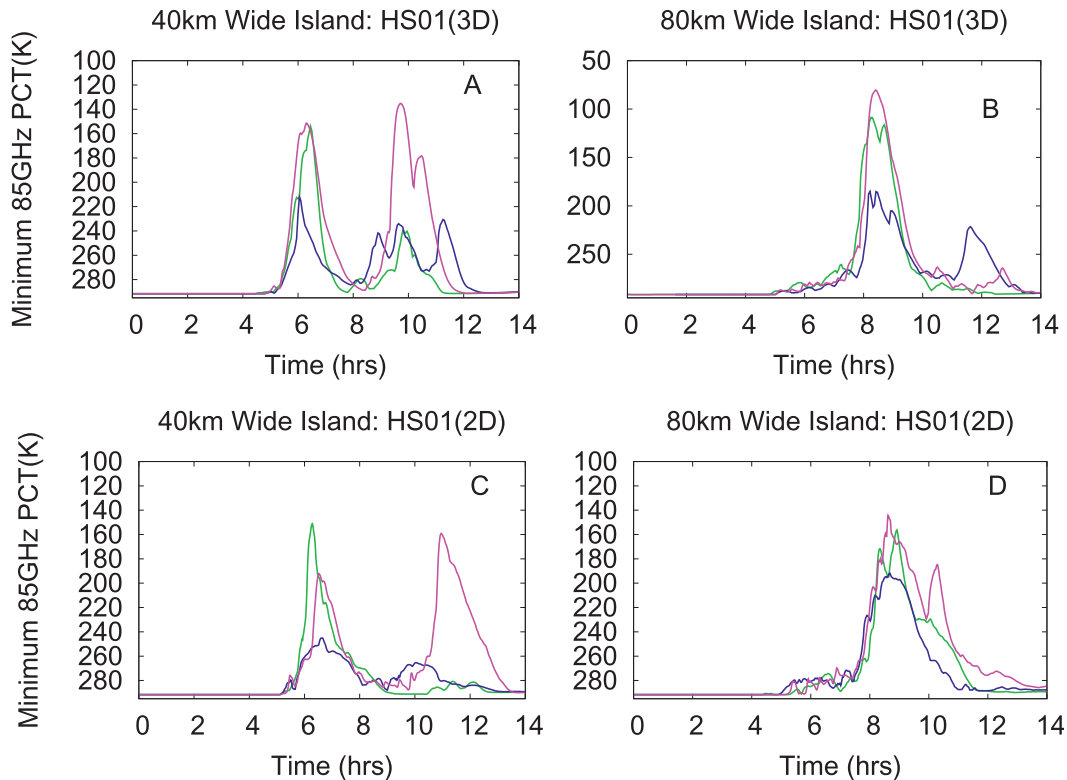


FIG. 7. Minimum 85-GHz PCT vs time for four simulations with Lin (green), Morrison (pink), and Thompson (blue) microphysics parameterizations. In each case the sounding is HS01. The 3D simulations of (a) a 40-km and (b) an 80-km island; (c), (d) are for corresponding 2D simulations. The two peaks in (a)–(c) correspond to an initial and second burst of convection due to two front-collision events (see text).

We examine this further in Fig. 6b, which shows regression fits to the 37–85-GHz relationship for a number of different 37-GHz windows. This comparison reveals that a window size near 15–20 km would match the data best. While the comparison shown is for the 80-km heating and HS01 sounding, behavior is similar in other cases. In the rest of the paper all of the 2D runs use the original 10-km and 4-km footprints for simulating the 37- and 85-GHz channels, respectively; thus, there will be a low bias in 37-GHz PCT.

c. Sensitivity to the microphysics scheme

The four panels in Fig. 7 show the time series of minimum 85-GHz PCT simulated with the three microphysical schemes (Morrison et al., Thompson, and Lin et al.) for 40- and 80-km “island” hot spots with 3D and 2D model setups. All are based on the HS01 sounding, chosen as a representative one that produces intermediate convective intensity.

Over the smaller island, two bursts of convection occur regardless of microphysical scheme or model dimension (although the second peak is very weak with

the Lin scheme in 2D). Inspection of movies (<http://www.astro.yale.edu/marjf>) made of the storms shows that the initial burst occurs when coastal fronts collide near the center of the domain. This storm generates fronts that reflect or trigger new fronts upon reaching the coasts, and these secondary fronts collide in a second storm (independent of domain size, not shown). With the Morrison scheme this second burst is as strong as or stronger than the first one, while with the other schemes it is weaker. Overall, for the smaller islands, the Lin and Morrison schemes produce significantly stronger convective signatures than the Thompson scheme in both 2D and 3D. We discuss this further in section 5b.

Over the larger island there is only one convective burst, apparently because the solar heating has weakened by the time when the second set of fronts arrives (later due to the larger island). Convection is stronger regardless of microphysical scheme or model dimension. The microphysical scheme has somewhat less impact on this than it had for the smaller island; this is probably because the smaller island is barely large enough to drive a strong response (see below).

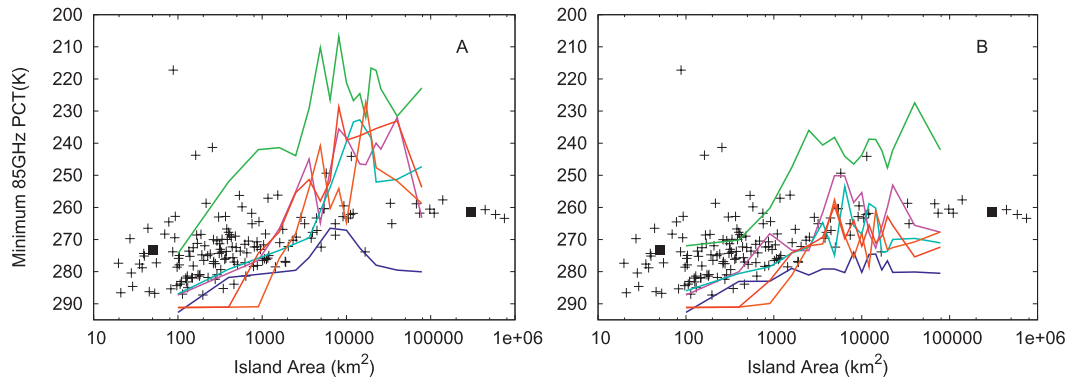


FIG. 8. Minimum 85-GHz PCT vs island/heated area. The average afternoon TRMM value for each island is shown by a plus sign. The filled boxes on the left and right of each panel are average TRMM values for ocean and land. The solid lines are 2D WRF simulations for the six different soundings (HIRH: green, LOWRH: dark blue, HS01: pink, LS01: orange, HS06: light blue, and HS06: red) vs island area, using (a) Morrison or (b) Thompson microphysics.

These comparisons confirm that the WRF-SDSU setup produces plausible simulations of the TRMM microwave PCT minima and radar height maxima in either 2D or 3D, although the simulated radiometric signatures are sensitive to initial sounding, model setup, and assumed beam footprints. We now examine a larger suite of 2D simulations, for heating widths ranging from 10 to 280 km, to determine the systematic changes that accompany larger regions of surface heating. As this required a large number of simulations, we performed these for the Thompson and Morrison schemes but not for the older Lin scheme.

5. Results: Trends of storm intensity with island size

a. TRMM intensity measures

To summarize the behavior over a single island or heating width and usefully compare simulations to observations, we average our three observable quantities over all relevant times during a WRF simulation. For the TRMM data we calculate a mean for each island and for WRF+SDSU one for each simulation (see section 3d). The resulting behaviors versus island area appear in Fig. 8. Here, “island area” is defined as the square of the heating width for simulations and as the measured surface area for real islands.

This figure shows that model results vary significantly with the initial sounding. To make a more precise comparison of the systematic behavior we show the grand mean of the simulations over all soundings in Fig. 9. This figure compares afternoon and all-day results from TRMM data and compares simulated results between the two microphysical schemes.

All three measures of convective strength grow stronger over larger islands, at a similar rate in both observations and simulations. In the 85-GHz and radar data, the “continental effect” (change between large and small islands) is comparable to or larger than the spread in model or observed results for a given island or heating size. The model agreement is fairly good despite the omission here of terrain effects (which are likely significant for some of the islands) and other continental influences.

The data show that all measures of convective strength have reached, or exceeded, their continental values by the time island size reaches roughly 10 000 km². There is a hint of a peak near this size in the simulations, but it is not as clear as the peak found by RSL08 and is not really evident in the data at all although there is a clear flattening of the curves above 10 000 km² (see section 6 for further discussion).

The two microphysical schemes produce similar trends but different means, especially in the case of the peak 40-dBZ reflectivity height where the Thompson scheme falls well below the observations, but the Morrison scheme is correct on average. That this variable is often zero, since only the strongest updrafts produce any 40-dBZ echoes, is somewhat problematic for computing means. Nonetheless, the very different amounts of graupel produced in the Thompson and Morrison schemes are probably the main reason for their different SDSU output. Morrison is also stronger than Thompson in the PCT measures, though this difference is smaller than the continental effect, especially for 85 GHz. For 85 GHz, the Thompson results match the observations whereas the Morrison PCTs are too low.

The simulated trends from small to 10 000 km² sizes are generally stronger in the simulations than the

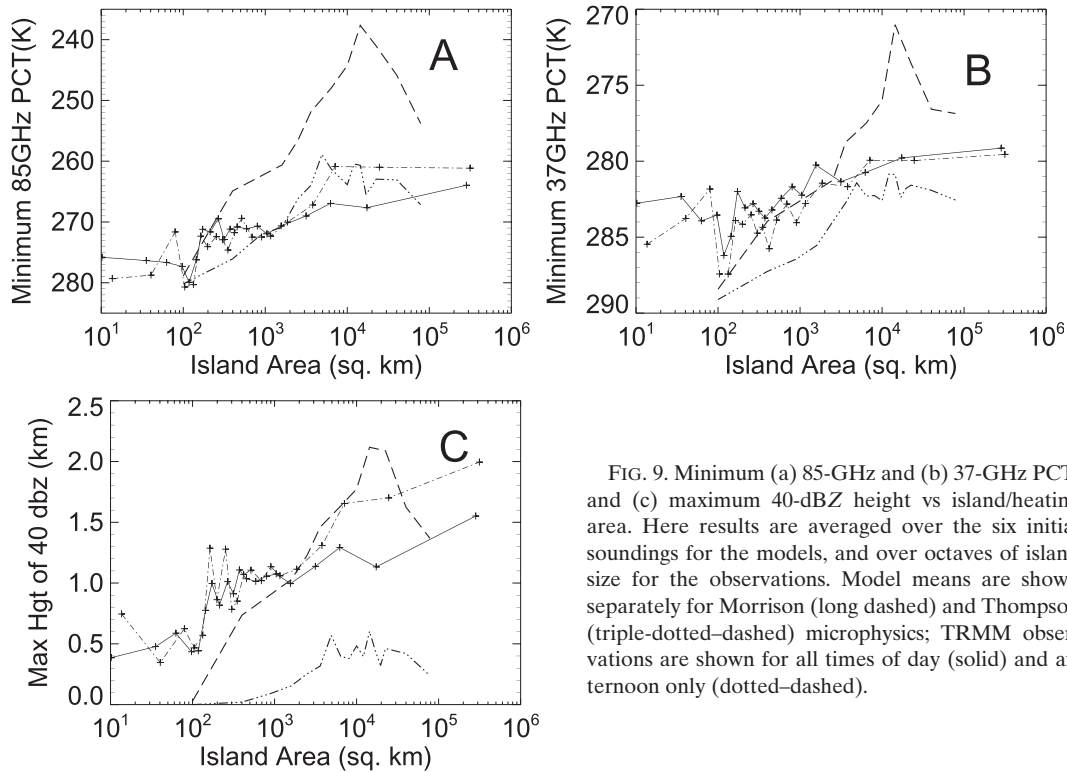


FIG. 9. Minimum (a) 85-GHz and (b) 37-GHz PCT, and (c) maximum 40-dBZ height vs island/heating area. Here results are averaged over the six initial soundings for the models, and over octaves of island size for the observations. Model means are shown separately for Morrison (long dashed) and Thompson (triple-dotted-dashed) microphysics; TRMM observations are shown for all times of day (solid) and afternoon only (dotted-dashed).

observations, by up to a factor of 2 or so for some measures with the Morrison scheme. The difference between afternoon and all-times TRMM data appears to be too small for this discrepancy to be explained by nonlocally generated storms in the observations. However, the simulated storms decrease somewhat in intensity between $10\,000\text{ km}^2$ and at the largest scales, so, if the continental effect is measured as the difference between small islands and the largest scale, the simulated and observed continental effects are reasonably close. Viewing it this way, the chief model-observational discrepancy would be the presence of a slight peak in intensity (as reported by RSL08) near $10\,000\text{ km}^2$ in simulations that is absent in observations (see section 6 for further discussion).

b. Other simulated quantities

Some insight into the above results may be gained by examining additional model quantities. Trends in graupel and rain mixing ratios, cloud height, minimum surface pressure perturbation (i.e., maximum surface pressure depression), and vertical velocity are shown in Figs. 10 and 11.

Figure 10 shows that the radiometric/TRMM intensity measures resemble the graupel concentrations (Fig. 10a) and are broadly reflected in cloud height variations (Fig. 10c). The graupel amounts are particularly

sensitive to input sounding, and for the LOWRH (dark blue) sounding graupel is only produced for island sizes from about $4\,000$ to $20\,000\text{ km}^2$, and cloud heights are quite low outside this size range. Twice as much graupel is produced by the Morrison as the Thompson scheme, for all sizes. The other frozen species, snow and cloud ice (not shown), show variations qualitatively resembling those of graupel.

Turning to indicators of storm dynamics (Fig. 11), the trend with island size remains striking while the impact of microphysical schemes and input soundings decreases significantly by comparison. The updrafts with Morrison microphysics are only slightly stronger (up to 2 m s^{-1} for some sizes, no difference for others) and the surface pressure low slightly deeper (by at most 25 Pa) than for Thompson. These effects of the microphysical scheme are about an order of magnitude smaller than the continental effect in each case. We infer from these results that microphysical impacts, whether through the scheme or the environmental humidity, affect the storm through altering the hydrometeor properties but with only modest impacts on storm dynamics. The rain mixing ratio (Fig. 10b) is enigmatic, however, as it is significantly affected by the microphysical scheme (about 30% less rain mixing ratio in Thompson) but little affected by the initial sounding. Both TRMM and SDSU-WRF also show a similar trend in storm raining area with island size (not shown).

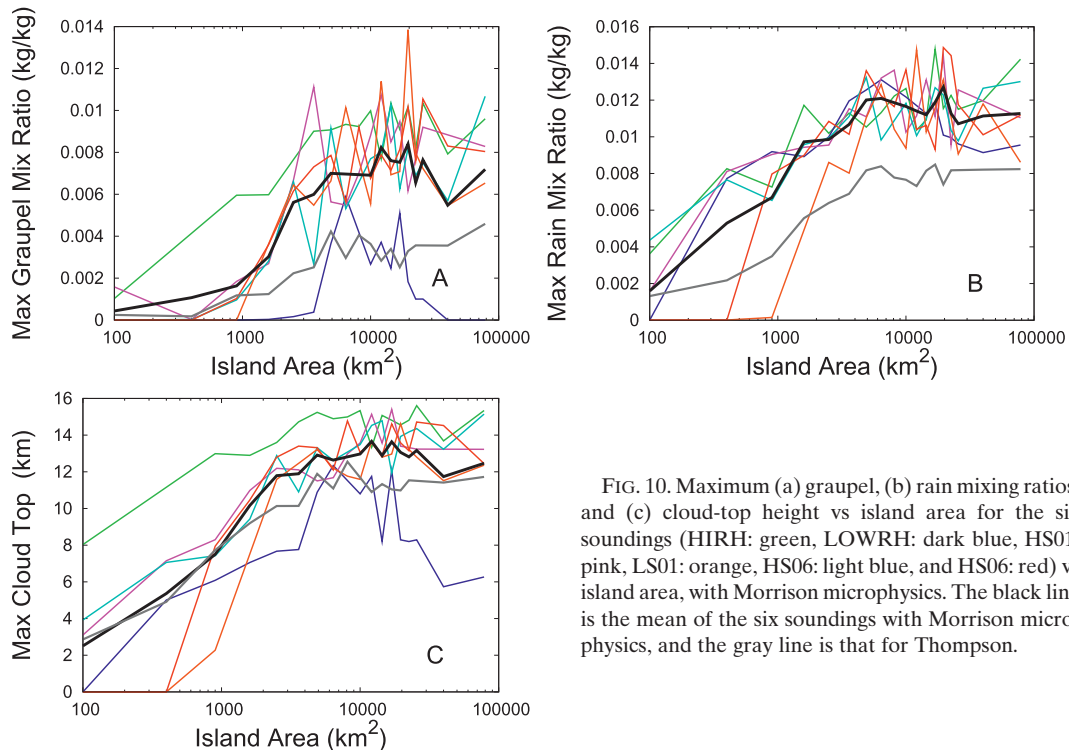


FIG. 10. Maximum (a) graupel, (b) rain mixing ratios, and (c) cloud-top height vs island area for the six soundings (HIRH: green, LOWRH: dark blue, HS01: pink, LS01: orange, HS06: light blue, and HS06: red) vs island area, with Morrison microphysics. The black line is the mean of the six soundings with Morrison microphysics, and the gray line is that for Thompson.

In the current setup, the peak CAPE values (averaged over the island) range from about 100–600 J kg⁻¹ for the smallest islands (depending on which sounding is used) to about 200–800 J kg⁻¹ for the largest. In similar simulations by Robinson and Sherwood (2006), increasing CAPE from 900 to 1500 J kg⁻¹ increased the maximum updraft speed from 24 to 32 m s⁻¹.⁴

That suggests that the approximate 200 J kg⁻¹ increase in CAPE from small to large islands found here is not a dominant cause of the 10 m s⁻¹ change from small to large islands. More significantly, if CAPE were the primary indicator of convective strength, then the 500 J kg⁻¹ increase in peak CAPE between the LOWRH and HIRH soundings (not shown) should have produced a corresponding increase in maximum updraft speed of about 10 m s⁻¹. However, Fig. 11b does not show any such increase. Both results imply that CAPE has little influence on updraft speed in the current setup.

6. Discussion: Comparison with RSL08

Previous studies have shown that local maxima in convective intensity often occur over mesoscale orographic

features (Toth and Johnson 1985) or islands (Simpson et al. 1993). RSL08 showed that a maximum in convective intensity should be expected over mesoscale heated regions even in the absence of effects from surface roughness or orography, or any differences in the atmospheric sounding. This response was due to basic dry dynamics in the presence of a preferred time and vertical scale for the heating. Convective responses decreased rapidly at scales below optimum, and very gently at scales above optimum. The optimum forcing was a Gaussian with a full width at half maximum of 50 km.

In the current study the maximum occurs closer to 100 km. To examine this, consider the parameters that determine the resonance scale according to RSL08: the depth of heated boundary layer H , the background static stability, and the heating ramp-up time scale T , which RSL08 argued was set by the time required for deep convection to develop (measured by the time from the start of the simulation to the moment of maximum CAPE).

While the static stability is about the same in the two studies, the other two parameters were not. The heated layer depth H (at time of maximum CAPE) was about 1 km in the simulations reported by RSL08, but only about 0.5 km in the simulations presented here. This may be because of RSL08 heating the lowest atmospheric levels directly (which we do not), changes in the model grid, or the use of different initial soundings. Further, in the RSL08 simulations the peak CAPE was reached after

⁴ Note that in Robinson and Sherwood (2006) the actual CAPE values were 1000 J kg⁻¹ less than reported due to the mistaken inclusion of latent heat of fusion when computing CAPE even though the simulations themselves did not include the freezing of condensate.

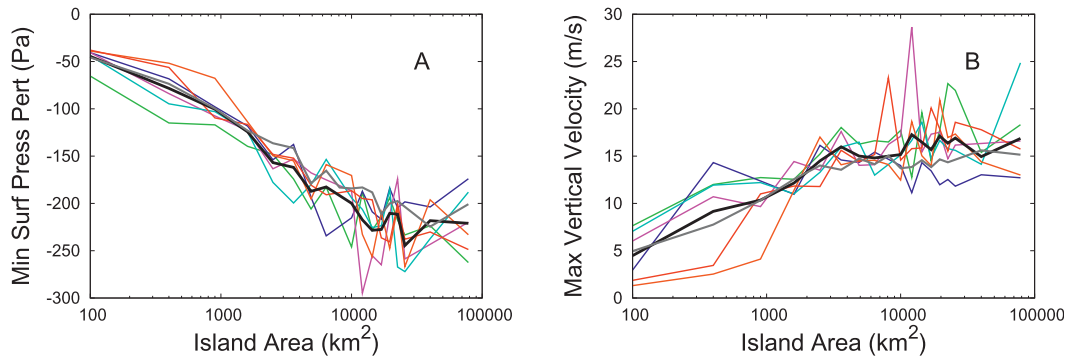


FIG. 11. As in Fig. 10, but for (a) minimum surface pressure perturbation and (b) maximum vertical velocity.

only 40 min, while in the current simulations it takes about 3 h. This difference probably arises from the same factors, plus the use of a slower (more realistic) heating rate. With H about half and T about quadruple the RSL08 values, linear theory would predict a resonance scale of around 100 km in the new simulations, as indeed shown by our trend results. Again, this can only be a rough comparison owing to the inexact quantification of the time scale and the heated layer depth H .

The rolloff at larger scales reported by RSL08, which they argued was caused by exceeding a resonant scale in the linear dynamics, appears more ambiguous here. There is indeed a marked peak in the LOWRH runs, which produced the weakest storms (Figs. 10a,c), but with the other initial soundings the storm strength remains roughly constant above 10 000 km². The reasons for this—in particular, the surprising dependence on input sounding—are not clear. As mentioned previously, there is little, if any, rolloff evident in the observations either. That is not too surprising, however, since real islands are not uniform and large land areas would typically have variations in surface characteristics on a range of scales including those on the order of 100 km. Hence we might expect any real landmass larger than the resonant scale to produce similarly strong convection. Another factor important in the real world is orography, which appears to shift the trend curve (this will be discussed in another article) but was not included in our simulations.

Finally, we have ignored the role of low-level advection, which was absent in RSL08 and is not particularly strong in the soundings used here. It is likely that the weak response simulated and observed over small islands is due not only to their inability to excite sufficiently deep waves but also to the loss of heat by advection offshore.

7. Conclusions

This study uses islands of various sizes as boundary conditions to test the ability of a cloud-resolving model

to simulate systematic changes in observed behavior under changed forcing. In short, we find that the WRF CRM is indeed able to simulate the observed trends in the key severity measures obtainable from space, and therefore the overall land–ocean difference. The increase in convective intensity going from small to largest islands, termed here the “continental effect,” is reproduced to an accuracy of perhaps 30% or better for all three measures of intensity considered: minimum 37- and 85-GHz polarization-corrected brightness temperatures and maximum height of 40-dBZ radar reflectivity. These measures correlate well in the model with graupel and snow amounts, peak updraft velocities, and greatest depth of the surface pressure heat low that drives low-level convergence into the storm.

We also investigated several practical issues, including the ability to use satellite simulators on two-dimensional model simulations, and found that these issues are manageable. The ability to use 2D simulations is valuable owing to the large number of runs required to reveal systematic changes in behavior that can be attributed to external forcings, due in turn both to the large variability in results for a given initial condition and the large range of initial conditions that may occur in nature. While individual simulations are sensitive to microphysical scheme and (to a somewhat lesser extent) model dimension and resolution, systematic trends do not appear to be nearly as sensitive to these, such that forced trends easily stand out. Our results thus support the use of 2D models to affordably perform large ensembles of runs when 3D dynamical effects are not deemed crucial to the phenomena under study, as argued by some other authors (e.g., C.-M. Wu et al. 2009).

The simulations reported here showed realistic trends despite identical initial temperature and humidity sounding, no differences in boundary layer thickness, no aerosol effects, and no differences in surface roughness or orography. The heat low also correlates well with simulated storm severity, yet is essentially a mesoscale feature. Our results therefore strengthen the suggestion of RSL08 that linear

mesoscale wave dynamics may be the dominant reason for the augmentation of convective strength over larger islands, and confirm observationally that the behavior over the smallest and largest islands smoothly approaches that over oceans and continents, respectively. Although horizontal advection of boundary layer air may have contributed to the trends simulated in the present study, winds were not strong, and RSL08 obtained similar results without this effect, suggesting it is not a crucial factor. Nonetheless, our results could be affected by the neglect of orography or other land influences, and by the fact that our chosen suite of initial soundings does not fully capture the range of environmental conditions such as strong surface winds.

One hallmark of the resonant behavior noted by RSL08 is the gentle rolloff of convective intensity above the resonant scale near 50 km. This was more ambiguous in the present simulations in that it depended on initial sounding; it also occurred at a resonant island width closer to 100 km, but for reasons that appear consistent with the basic theory. This rolloff is weak or absent in TRMM observations, but that could be expected owing to the irregularities of real islands. In particular, convection might remain strong over arbitrarily large actual landmasses due to mesoscale variations in surface conditions, which could excite any resonances at scales smaller than the landmass itself but were absent in the simulations. The hypothesis that mesoscale interior surface variability is responsible for the intensity of continental convection deserves further study but has observational support (Nesbitt and Anders 2009; Toth and Johnson 1985). We also have neglected orography and the irregular shape of real islands.

While our results are qualitatively supported by a few three-dimensional simulations, it is possible that detailed results will differ when 3D behavior is included. They may also be sensitive to resolution, which was not thoroughly checked. While we did not find that 3D cloud-scale behavior made a significant difference, we did find that simulated storm severities are quite sensitive to, among other things, the shape of islands in three dimensions. This will complicate idealized studies in three dimensions and is worthy of further investigation.

Acknowledgments. This work was supported by the NSF Physical and Dynamical Meteorology program, Grant DYN078550. The computational component of this work was supported in part by the facilities and staff of the Yale University Faculty of Arts and Sciences High Performance Computing Center.

REFERENCES

- Arakawa, A., 2004: The cumulus parameterization problem: Past, present, and future. *J. Climate*, **17**, 2493–2525.
- Avissar, R., and Y. Liu, 1996: Three-dimensional numerical study of shallow convective clouds and precipitation induced by land surface forcing. *J. Geophys. Res.*, **101**, 7499–7518.
- Bacmeister, J. T., M. J. Suarez, and F. R. Robertson, 2006: Rain reevaporation, boundary layer–convection interactions, and Pacific rainfall patterns in an AGCM. *J. Atmos. Sci.*, **63**, 3383–3403.
- Brooks, H. E., 2009: Proximity soundings for severe convection for Europe and the United States from reanalysis data. *Atmos. Res.*, **93**, 546–553.
- Carbone, R., J. Wilson, T. D. Keenan, and J. Hacker, 2000: Tropical island convection in the absence of significant topography. Part I: Life cycle of diurnally forced convection. *Mon. Wea. Rev.*, **128**, 3459–3480.
- Chemel, C., M. Russo, J. Pyle, R. Sokhi, and C. Schiller, 2009: Quantifying the imprint of a severe Hector thunderstorm during ACTIVE/SCOUT-O3 onto the water content in the upper troposphere/lower stratosphere. *Mon. Wea. Rev.*, **137**, 2493–2514.
- Connolly, P., T. Choularton, M. Gallagher, K. Bower, M. Flynn, and J. Whiteway, 2006: Cloud-resolving simulations of intense tropical Hector thunderstorms: Implications for aerosol–cloud interactions. *Quart. J. Roy. Meteor. Soc.*, **132**, 3079–3106.
- Crook, N., 2000: Understanding Hector: The dynamics of island thunderstorms. *Mon. Wea. Rev.*, **129**, 1550–1563.
- Dahl, A. L., 1986: *Review of the Protected Areas System in Oceania*. International Union for Conservation of Nature and Natural Resources, 239 pp.
- , 1991: *Island Directory: UNEP Regional Seas*. Directories and Bibliographies Series, No. 35, United Nations Environment Programme, 573 pp.
- Fritsch, J. M., and R. E. Carbone, 2004: Improving quantitative precipitation forecasts in the warm season: A USWRP research and development strategy. *Bull. Amer. Meteor. Soc.*, **85**, 955–965.
- Heymsfield, A. J., and C. M. R. Platt, 1984: A parameterization of the particle size spectrum of ice clouds in terms of the ambient temperature and the ice water content. *J. Atmos. Sci.*, **41**, 846–855.
- Holloway, C. E., and J. D. Neelin, 2009: Moisture vertical structure, column water vapor, and tropical deep convection. *J. Atmos. Sci.*, **66**, 1665–1683.
- Iguchi, T., T. Kozu, R. Meneghini, J. Awaka, and K. Okamoto, 2000: Rain-profiling algorithm for the TRMM precipitation radar. *J. Appl. Meteor.*, **39**, 2038–2052.
- Inoue, T., M. Satoh, Y. Hagihara, H. Miura, and J. Schmetz, 2010: Comparison of high-level clouds represented in a global cloud system–resolving model with CALIPSO/CloudSat and geostationary satellite observations. *J. Geophys. Res.*, **115**, D00H22, doi:10.1029/2009JD012371.
- Khain, A. P., and B. Lynn, 2009: Simulation of a supercell storm in clean and dirty atmosphere using weather research and forecasting model with spectral bin microphysics. *Geophys. Res. Lett.*, **114**, D19209, doi:10.1029/2009JD011827.
- Kingsmill, D., 1995: Convection initiation associated with a sea-breeze front, a gust front, and their collision. *Mon. Wea. Rev.*, **123**, 2913–2933.
- Kirshbaum, D., and R. Smith, 2009: Orographic precipitation in the tropics: Large-eddy simulations and theory. *J. Atmos. Sci.*, **66**, 2559–2578.
- Kummerow, C., 1993: On the accuracy of the Eddington approximation for radiative transfer in the microwave frequencies. *J. Geophys. Res.*, **98**, 2757–2765.

- , W. Barnes, T. Kozu, J. Shiue, and J. Simpson, 1998: The Tropical Rainfall Measuring Mission (TRMM) sensor package. *J. Atmos. Oceanic Technol.*, **15**, 809–817.
- Li, X., W.-K. Tao, A. P. Khain, J. Simpson, and D. E. Johnson, 2009: Sensitivity of a cloud-resolving model to bulk and explicit bin microphysical schemes. Part I: Comparisons. *J. Atmos. Sci.*, **66**, 3–21.
- Li, Y., E. J. Zipser, S. K. Krueger, and M. A. Zulauf, 2008: Cloud-resolving modeling of deep convection during KWAJEX. Part I: Comparison to TRMM satellite and ground-based radar observations. *Mon. Wea. Rev.*, **136**, 2699–2712.
- Lima, M. A., and J. W. Wilson, 2008: Convective storm initiation in a moist tropical environment. *Mon. Wea. Rev.*, **136**, 1847–1864.
- Lin, Y.-L., R. Farley, and H. Orville, 1983: Bulk parameterization of the snow field in a cloud model. *J. Climate Appl. Meteor.*, **22**, 1065–1092.
- Liu, C., E. J. Zipser, D. J. Cecil, S. W. Nesbitt, and S. Sherwood, 2008: A cloud and precipitation feature database from nine years of TRMM observations. *J. Appl. Meteor. Climatol.*, **47**, 2712–2728.
- Marchand, R., N. Beagley, and T. P. Ackerman, 2009a: Evaluation of hydrometeor occurrence profiles in the multiscale modeling framework climate model using atmospheric classification. *J. Climate*, **22**, 4557–4573.
- , J. Haynes, G. G. Mace, T. Ackerman, and G. Stephens, 2009b: A comparison of simulated cloud radar output from the multiscale modeling framework global climate model with CloudSat cloud radar observations. *J. Geophys. Res.*, **114**, D00A20, doi:10.1029/2008JD009790.
- Masunaga, H., and C. D. Kummerow, 2005: Combined radar and radiometer analysis of precipitation profiles for a parametric retrieval algorithm. *J. Atmos. Oceanic Technol.*, **22**, 909–929.
- , and Coauthors, 2010: Satellite Data Simulator Unit: A multisensor, multispectral satellite simulator package. *Bull. Amer. Meteor. Soc.*, **91**, 1625–1632.
- Matsui, T., X. Zeng, and W.-K. Tao, 1989: Precipitation retrieval over land and ocean with the SSM/I: Identification and characteristics of the scattering signal. *J. Atmos. Oceanic Technol.*, **6**, 254–273.
- May, P. T., G. Allen, G. Vaughan, and P. Connolly, 2009: Aerosol and thermodynamic effects on tropical cloud systems during TWICE and ACTIVE. *Atmos. Chem. Phys.*, **9**, 15–24.
- Moncrieff, M. W., and J. S. A. Green, 1972: The propagation and transfer properties of steady convective overturning in shear. *Quart. J. Roy. Meteor. Soc.*, **98**, 336–352.
- Morrison, H., and J. Pinto, 2005: Mesoscale modeling of springtime Arctic mixed-phase stratiform clouds using a new two-moment bulk microphysics scheme. *J. Atmos. Sci.*, **62**, 3683–3704.
- , G. Thompson, and V. Tatarskii, 2009: Impact of cloud microphysics on the development of trailing stratiform precipitation in a simulated squall line: Comparison of one- and two-moment schemes. *Mon. Wea. Rev.*, **137**, 991–1007.
- Nesbitt, S. W., and A. M. Anders, 2009: Very high resolution precipitation climatologies from the Tropical Rainfall Measuring Mission precipitation radar. *Geophys. Res. Lett.*, **36**, L15815, doi:10.1029/2009GL038026.
- Petch, J. C., P. N. Blossey, and C. S. Bretherton, 2008: Differences in the lower troposphere in two- and three-dimensional cloud-resolving model simulations of deep convection. *Quart. J. Roy. Meteor. Soc.*, **134**, 1941–1946.
- Pritchard, M. S., and R. C. J. Somerville, 2008: Empirical orthogonal function analysis of the diurnal cycle of precipitation in a multi-scale climate model. *Geophys. Res. Lett.*, **36**, L05812, doi:10.1029/2008GL036964.
- Robinson, F., and S. Sherwood, 2006: Modeling the impact of convective entrainment on the tropical tropopause. *J. Atmos. Sci.*, **63**, 1013–1027.
- , —, and Y. Li, 2008: Resonant response of deep convection to surface hot spots. *J. Atmos. Sci.*, **65**, 276–286.
- Saito, K., T. Keenan, G. Holland, and K. Puri, 2001: Numerical simulation of the diurnal evolution of tropical island convection over the maritime continent. *Mon. Wea. Rev.*, **129**, 378–400.
- Schafer, R., P. May, T. Keenan, K. McGuffie, W. Ecklund, P. Johnston, and K. Gage, 2001: Boundary layer development over a tropical island during the Maritime Continent Thunderstorm Experiment. *J. Atmos. Sci.*, **58**, 2163–2179.
- Sherwood, S. C., V. T. J. Phillips, and J. S. Wettlaufer, 2006: Small ice crystals and the climatology of lightning. *Geophys. Res. Lett.*, **33**, L05804, doi:10.1029/2005GL025242.
- , R. Roca, T. M. Weckwerth, and N. G. Andronova, 2010: Tropospheric water vapor, convection and climate. *Rev. Geophys.*, **48**, RG2001, doi:10.1029/2009RG000301.
- Simpson, J., T. D. Keenan, B. Ferrier, R. H. Simpson, and G. J. Holland, 1993: Cumulus mergers in the Maritime Continent region. *Meteor. Atmos. Phys.*, **51**, 73–99.
- Skamarock, W. C., and Coauthors, 2008: A description of the Advanced Research WRF, version 3. NCAR Tech. Note NCAR/TN-475+STR, 113 pp. [Available online at http://www.mmm.ucar.edu/wrf/users/docs/arw_v3.pdf.]
- Smolarkiewicz, P. K., R. Rasmussen, and T. Clark, 1988: On the dynamics of Hawaiian cloud bands: Island forcing. *J. Atmos. Sci.*, **45**, 1872–1905.
- Soong, S.-T., and Y. Ogura, 1980: Response of tradewind cumuli to large-scale processes. *J. Atmos. Sci.*, **37**, 2035–2050.
- Spencer, R., H. Goodman, and R. E. Hood, 1989: Precipitation retrieval over land and ocean with the SSM/I: Identification and characteristics of the scattering signal. *J. Atmos. Oceanic Technol.*, **6**, 254–273.
- Stan, C., C. Khairoutdinov, C. DeMott, V. Krishnamurthy, D. Straus, D. Randall, J. Kinter, and J. Shukla, 2010: An ocean-atmosphere climate simulation with an embedded cloud-resolving model. *Geophys. Res. Lett.*, **37**, L01702, doi:10.1029/2009GL040822.
- Stevens, B., 2005: Atmospheric moist convection. *Annu. Rev. Earth Planet. Sci.*, **33**, 605–643.
- Thompson, G., R. Rasmussen, and K. Manning, 2004: Explicit forecasts of winter precipitation using an improved bulk microphysics scheme: Part I: Description and sensitivity analysis. *Mon. Wea. Rev.*, **132**, 519–542.
- Toth, J. J., and R. H. Johnson, 1985: Summer surface flow characteristics over northeast Colorado. *Mon. Wea. Rev.*, **113**, 1458–1469.
- Wakimoto, R. M., and H. V. Murphey, 2008: Airborne Doppler radar and sounding analysis of an oceanic cold front. *Mon. Wea. Rev.*, **136**, 1475–1491.
- Williams, E., and S. Stanfill, 2002: The physical origin of the land-ocean contrast in lightning activity. *C. R. Phys.*, **3**, 1277–1292.
- Wilson, J. W., and W. E. Schreiber, 1986: Initiation of convective storms at radar-observed boundary-layer convergence lines. *Mon. Wea. Rev.*, **114**, 2516–2536.
- Wissmeier, U., and R. Goler, 2009: A comparison of tropical and midlatitude thunderstorm evolution in response to wind shear. *J. Atmos. Sci.*, **66**, 2385–2401.
- Wu, C.-M., B. Stevens, and A. Arakawa, 2009: What controls the transition from shallow to deep convection? *J. Atmos. Sci.*, **66**, 1793–1806.

- Wu, J., A. Del Genio, M.-S. Yao, and A. B. Wolf, 2009: WRF and GISS SCM simulations of convective updraft properties during TWP-ICE. *J. Geophys. Res.*, **114**, D04206, doi:10.1029/2008JD010851.
- Xu, K. M., and Coauthors, 2002: An intercomparison of cloud-resolving models with the Atmospheric Radiation Measurement summer 1997 intensive observation period data. *Quart. J. Roy. Meteor. Soc.*, **128**, 593–624.
- Yu, C.-K., and L.-W. Cheng, 2008: Radar observations of intense orographic precipitation associated with Typhoon Xangsane (2000). *Mon. Wea. Rev.*, **136**, 497–521.
- Zhang, X. H., W. Y. Lin, and M. H. Zhang, 2007: Toward understanding the double intertropical convergence zone pathology in coupled ocean–atmosphere general circulation models. *J. Geophys. Res.*, **112**, D12102, doi:10.1029/2006JD007878.
- Zhang, Y., and Coauthors, 2008: On the diurnal cycle of deep convection, high-level cloud, and upper troposphere water vapor in the multiscale modeling framework. *J. Geophys. Res.*, **113**, D16105, doi:10.1029/2008JD009905.
- Zhou, Y. P., and Coauthors, 2007: Use of high-resolution satellite observations to evaluate cloud and precipitation statistics from cloud-resolving model simulations. Part I: South China Sea Monsoon Experiment. *J. Atmos. Sci.*, **64**, 4309–4329.
- Zipser, E. J., and K. R. Lutz, 1994: The vertical profile of radar reflectivity of convective cells: A strong indicator of storm intensity and lightning probability? *Mon. Wea. Rev.*, **122**, 1751–1759.
- , D. J. Cecil, C. T. Liu, S. W. Nesbitt, and D. P. Yorty, 2006: Where are the most intense thunderstorms on earth? *Bull. Amer. Meteor. Soc.*, **87**, 1057–1071.